UCLA

Title

Optogenetic fMRI and electrophysiological identification of region-specific connectivity between the cerebellar cortex and forebrain.

Permalink

https://escholarship.org/uc/item/4m06b3gg

Authors

Choe, Katrina Y
Sanchez, Carlos F
Harris, Neil G
et al.

Publication Date

2018-06-01

DOI

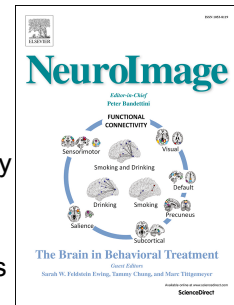10.1016/j.neuroimage.2018.02.047

Copyright Information

Peer reviewed

Accepted Manuscript

Optogenetic fMRI and electrophysiological identification of region-specific connectivity between the cerebellar cortex and forebrain

Katrina Y. Choe, Carlos F. Sanchez, Neil G. Harris, Thomas S. Otis, Paul J. Mathews

Please cite this article as: Choe, K.Y., Sanchez, C.F., Harris, N.G., Otis, T.S., Mathews, P.J., Optogenetic fMRI and electrophysiological identification of region-specific connectivity between the cerebellar cortex and forebrain, *NeuroImage* (2018), doi: 10.1016/j.neuroimage.2018.02.047.

Optogenetic fMRI and electrophysiological identification of region-specific connectivity between the cerebellar cortex and forebrain

Katrina Y. Choe[a,b], Carlos F. Sanchez[e], Neil G. Harris[c], Thomas S. Otis[d], and Paul J. Mathews[b,e,f,*]

a- Semel Institute for Neuroscience and Human Behavior, University of California at Los Angeles, Los Angeles, CA 90095, USA.
b- Integrative Center for Learning and Memory, University of California at Los Angeles, Los Angeles, CA 90095, USA.
c- The UCLA Brain Injury Research Center, Department of Neurosurgery, David Geffen School of Medicine at the University of California at Los Angeles, Los Angeles, CA 90095, USA.
d- Department of Neurobiology, David Geffen School of Medicine, University of California at Los Angeles, Los Angeles, Los Angeles, CA 90095, USA.
e- Los Angeles Biomedical Research Institute at Harbor-UCLA Medical Center, Torrance, CA, 90502 USA.
f- Department of Neurology, David Geffen School of Medicine, University of California at Los Angeles, Los Angeles, CA 90095, USA.
*- Corresponding Author

Correspondence to:

Paul J. Mathews, Ph.D.
LA BioMedical Research Institute (LA BioMed)
1124 W Carson St
Torrance, CA 90502
Ph: (310) 222-5693
pmathews@ucla.edu

Footnote:
Present address of Dr. Thomas Otis:
Sainsbury Wellcome Centre, University College London, 25 Howland St., London, U.K.

Abstract

Complex animal behavior is produced by dynamic interactions between discrete regions of the brain. As such, defining functional connections between brain regions is critical in gaining a full understanding of how the brain generates behavior. Evidence suggests that discrete regions of the cerebellar cortex functionally project to the forebrain, mediating long-range communication potentially important in motor and non-motor behaviors. However, the connectivity map remains largely incomplete owing to the challenge of driving both reliable and selective output from the cerebellar cortex, as well as the need for methods to detect region specific activation across the entire forebrain. Here we utilize a paired optogenetic and fMRI (ofMRI) approach to elucidate the downstream forebrain regions modulated by activating a region of the cerebellum that induces stereotypical, ipsilateral forelimb movements. We demonstrate with ofMRI, that activating this forelimb motor region of the cerebellar cortex results in functional activation of a variety of forebrain and midbrain areas of the brain, including the hippocampus and primary motor, retrosplenial and anterior cingulate cortices. We further validate these findings using optogenetic stimulation paired with multi-electrode array recordings and post-hoc staining for molecular markers of activated neurons (i.e. c-Fos). Together, these findings demonstrate that a single discrete region of the cerebellar cortex is capable of influencing motor output and the activity of a number of downstream forebrain as well as midbrain regions thought to be involved in different aspects of behavior.

INTRODUCTION

The cerebellum is believed to play a key role in the accurate timing of body movements necessary for balance and coordinated movements. Anatomical, physiological, and clinical evidence also implicates the cerebellum in non-motor behaviors, ranging from cognition to emotion (Adamaszek et al., 2017; Arrigo et al., 2014; Bostan et al., 2013; Buckner et al., 2011; Chen et al., 2014; Crippa et al., 2016; Ichinohe et al., 2000; Kelly and Strick, 2003; Kim et al., 1994; Middleton and Strick, 2001; Parker et al., 2017; Schmahmann et al., 2004). Its participation in both motor and non-motor behaviors is mediated through neural interactions between distinct anatomical regions of the cerebellum and areas throughout the forebrain, midbrain, brainstem, and spinal cord.

Similar to the neocortex, the cerebellar cortex is composed of a laminated structure that has a repeating motif of neuronal connections and contains multiple somatotopic representations of the body (Apps and Hawkes, 2009; Balsters et al., 2014; Grodd et al., 2001; Manni and Petrosini, 2004; Schlerf et al., 2010). Inputs to the cerebellar cortex carry information from across the body and the central nervous system, including externally (sensory and proprioceptive modalities) and internally (higher-order processing) generated signals (Huang et al., 2013). Upon reaching the cerebellar cortex, this information is parsed in an extensive input layer of granule cells and ultimately integrated within GABAergic Purkinje neurons. Maintaining high levels of spontaneous activity (40-100 Hz at rest), Purkinje neurons control cerebellar output by tonically inhibiting cerebellar output neurons located in the cerebellar nuclei (or vestibular nucleus in the case of the flocculus). In comparison to cerebellar inputs, the downstream outputs of the cerebellum targeting the forebrain are not well understood. Work employing multi-synaptic tracing methods in non-human primates and rodents have identified anatomical substrates connecting the cerebellum through the thalamus to several forebrain regions, including the motor, prefrontal, and parietal cortices (Akkal et al., 2007; Dum and Strick, 2003; Middleton and Strick, 2001). Consistent with the existence of such anatomical pathways, resting-state functional magnetic resonance imaging (fMRI) in humans has indicated functional connectivity between the cerebellar cortex and a large number of areas across the neocortex (Bernard et al., 2012; Buckner et al., 2011; Halko et al., 2014; Rastogi et al., 2015); however, it remains unknown whether these activity correlations represent the capacity of cerebellar output to drive changes in forebrain activity patterns. These observations have prompted new investigations focused on the details of connectivity of the cerebellum with the rest of the brain and the functional roles these connections play in specific aspects of motor and non-motor behaviors. To begin to attribute these functional roles to discrete cerebellar regions, we must first identify and map out where different parts of the cerebellar cortex can modulate forebrain as well as midbrain activity.

Constructing a functional map of cerebellum-to-forebrain connections poses a major technical challenge. For one, approaches like resting-state fMRI approaches lack directionality and rely on correlational rather than causal relationships. These shortcomings can be mitigated by activating stereotaxically-defined cerebellar regions to generate region-specific output, while assaying whole-brain activity using fMRI approaches. Unfortunately, traditional methods of activating local neuronal populations in the cerebellar cortex, like electrical stimulation or pharmacology, do not produce precise control over cerebellar output. This is because 1) Purkinje neurons inhibit the activity of cerebellar output neurons and thus exciting them can result in unpredictable changes in cerebellar output, and 2) electrical excitation can generate antidromic excitation of cerebellar afferents (e.g. pons and inferior olive). Integration of optogenetics and rodent fMRI allow us to directly overcome these challenges. The approach, termed optogenetic fMRI (ofMRI), entails acquisition of whole-brain fMRI data while using light to selectively activate or deactivate genetically-defined populations of neurons expressing light-sensitive opsins (Lee et al., 2010). To date, ofMRI has been utilized to identify and examine functional connections between multiple brain regions including the motor cortex, basal ganglia, prefrontal cortex, and hippocampus (Bernal-Casas et al., 2017; Chan et al., 2017; Ferenczi et al., 2016; Lee et al., 2016; Lee, 2012; Leong et al., 2016; Ryali et al., 2016; Weitz et al., 2015).

In prior work using optogenetics, we and others have shown that transiently silencing inhibitory Purkinje neurons with light stimulation triggers a burst of action potentials in downstream output neurons in the cerebellar nuclei to drive cerebellar output (Heiney et al., 2014; Lee et al., 2015). With this approach, discrete regions of the cerebellar cortex can be targeted by stereotaxically positioning optic fibers on or into the tissue, thereby providing a conduit with which to deliver precisely timed, transient pulses of light. Furthermore, unlike electrical stimulation or pharmacological manipulation, one can transiently silence neuronal activity using this method by shining light onto expressed opsins that are capable of hyperpolarizing neuronal membrane

potential. In a forelimb region of the cerebellar cortex, we have demonstrated that by optogenetically pausing otherwise tonically active Purkinje neurons, we can induce a specific pattern of short-latency forelimb movements (Lee et al., 2015). By performing whole-brain fMRI scans of mice while transiently silencing Purkinje neurons in the forelimb region of the cerebellar cortex, we show that output from this single cerebellar region can modulate activity in both putative motor and non-motor regions of the forebrain as a result of input from the cerebellum and/or feedback from forelimb movement. Furthermore, we confirm these findings using multi-electrode array recordings for a subset of the discovered regions and staining for neural activity markers (i.e. c-Fos). These results demonstrate the utility of the ofMRI approach in elucidating the functional activation of various forebrain and midbrain regions in response to output from a distinct region of the cerebellar cortex, and define potential functional pathways by which this area can manipulate activity across these regions.

MATERIALS AND METHODS

Mice

All animal procedures were performed in accordance with NIH standards and were approved by the University of California, Los Angeles and Los Angeles Biomedical Institute Institutional Animal Care and Use Committee. Mice homozygous for L7-Cre (B6;129-Tg(Pcp2-cre)2Mpin/J; The Jackson Laboratory: #004146) (Barski et al., 2000) were crossed with Rosa-CAG-LSL(RCL)-Arch-GFP mice (Ai35, B6;129S-Gt(ROSA)26Sortm35.1(CAG-aop3/GFP)Hze/ J, The Jackson Laboratory: 012569) (Madisen et al., 2012) to direct expression of Archaerhodopsin-GFP in L7-positive Purkinje neurons in the resulting offspring (Han et al., 2014; Nguyen-Vu et al., 2013). L7-cre hemizygotes or C57Bl/6 mice were used as experimental controls where specified. Different sets of mice were used for ofMRI, electrophysiological recordings, and immunohistochemical experiments. For ofMRI experiments two groups of mice were used, one for examination of frequency parameters, the other for examination of intensity parameters. Experiments to examine functional connectivity using 5 Hz, 20 mW for stimulation were pooled across animals from both the intensity and frequency groups. All animals in the ofMRI, electrophysiological recordings, and immunohistochemical experiments were examined for a forelimb motor response, but only a subset of ofMRI mice were used to measure motor behavior as head bars detached from the skull on some mice precluding placement in the behavioral recording apparatus.

Surgical Procedures

OfMRI: All surgical procedures were performed under isoflurane (1.5-2%) anesthesia, and performed at least 5 days prior to scanning. Animals were placed into a stereotaxic device (Kopf), and custom-designed 3D-printed head bars (Zortrax M200, Ahmanson-Lovelace Brain Mapping Center (ALBMC) at UCLA) were glued to the skull over Bregma using Vetbond (3M). A small craniotomy was made into the caudal side of the occipital bone. After stereotaxic positioning a 0.22 mm-diameter optic fiber cannula (Doric Lenses) was horizontally inserted through the craniotomy into the forelimb region of the cerebellum (X: 1.9 mm, Y: -6.25 mm, Z: 2 mm from Bregma, (Lee, 2012), and fixed into place using Metabond (Parkell) and dental cement (Bosworth).

Electrophysiology: Animals underwent two surgeries in which they were first anesthetized (isoflurane, 1.5-2%) and placed into a stereotaxic device. During the first surgery, a two-piece stainless steel head bar was Metabond-cemented to the lateral edges of the skull. In the exact same fashion as described above for the ofMRI experiments, an optic cannula was horizontally inserted into the cerebellum with the tip just adjacent to the forelimb region of the cerebellum. On the day of recording, animals underwent a second surgery for a craniotomy. An opening in the skull (~1.5 x 1.5 mm square) through which to insert the multi-electrode array was centered over motor cortex (X: 1 mm, Y: 0 mm) or the retrosplenial cortex (X: 0.5 mm, Y: 1.75 mm), the latter of which allowed us to also record from the hippocampus and dorsal thalamus when the electrode array was inserted more ventrally. Craniotomies were temporarily sealed over using a silicone elastomer (Kwik Kast, World Precision Instruments) for no less than 4 hours to allow for recovery from anesthesia.

Behavioral analysis

To confirm the effectiveness of laser stimulation in triggering forelimb movement, optogenetic activation of the cerebellar forelimb region and forelimb movement analysis were carried out in a subset of experimental mice with horizontal optic fiber placement (Arch: n=4, control: n=2), using a previously described method (Lee et al., 2015). Briefly, head-fixed animals were placed on a freely moving rotary disc (Ware Inc.). A TTL controlled 1W, 532 nm diode-pumped solid-state (DPSS, OptoEngine) laser coupled to a fiber optic patch cable (Thorlabs) was connected to the horizontal optic cannula affixed to the head of each mouse. Forelimb

movements were induced using light intensities of approximately 143 mW/mm^2 (equivalent to 20 mW from 200 µm-diameter fiber tip) pulsed at 5 Hz with a 50% duty cycle. Kinematic movements were measured offline using custom limb tracking software (Labview, National Instruments) and further analyzed in Excel (Microsoft) and Igor Pro 6 (Wavemetrics). Limb tracking captured movement in a 2-dimensional plane by measuring the position of an infrared reflective dot temporarily glued (Elmer's white) to the mouse's forepaw/wrist. Results from 8-16 trials were first averaged for each mouse; each experimental group then represents averages of such data from the indicated number of mice.

Magnetic resonance imaging and optogenetic stimulation of the cerebellum

The mouse to be scanned was first briefly anesthetized with 2% isoflurane vaporized in oxygen flowing at 1 L/min. After placement on an MRI-compatible cradle, a generous amount of artificial eye tear ointment (Akorn) as well as a 3 mm-thick agar gel cap (Sigma, 3% in distilled water) was placed over the head of the mouse, in order to reduce signal distortion in the blood-oxygen-level-dependent (BOLD) signal (Adamczak et al., 2010). Then, a 4-channel phased-array surface coil (Bruker) was placed on top of the gel cap. Finally, the whole assembly was secured to the cradle using a custom-designed 3D-printed head-bar and holder set (Zortrax M200, **Fig. S1**). To minimize time-dependent effects of the anesthetic on the BOLD signal, these initial steps were performed within a 10- to 15-minute time window (Magnuson et al., 2014). Following the protocol used in a previous publication (Adamczak et al., 2010), isoflurane was gradually discontinued and sedation was initiated with a single subcutaneous (s.c.) injection of dexmedetomidine (Dexdomitor®, Zoetis; 0.15 mg/kg) followed by continuous s.c. infusion at 0.3 mg/kg/hr throughout the duration of the imaging. Respiration and temperature of the mouse were continuously monitored remotely, and temperature was maintained in a physiological range (37 ± 1 °C; Small Animal Instruments Inc.) by a combination of a built-in warm circulated water in the MRI cradle coupled to a water heater pump and homeothermically-controlled forced warm air over the body (SA11 Instr, Inc., USA). At the end of the imaging session, a sedative reversal agent, atipamezole (Antisedan®, Pfizer) was administered at 1.5 mg/kg (i.p.).

Magnetic resonance imaging was performed using a 7 Tesla (T) Biospec small animal MRI system using Paravision 5.2 software (Bruker). Data were acquired using the S116 Bruker gradients (400 mT/m) in combination with a 4-channel surface receive-only coil (described above) and a 72 mm birdcage transmit coil. An initial series of scans was performed to confirm proper head position, then localized FASTMAP shimming was performed to improve field homogeneity. T2-weighted structural scans were acquired with a Rapid-Relaxation-with-Enhancement (RARE) sequence (RARE factor=8, Echo time (TE)=56 ms, repetition time (TR)=6,018 ms, 4 averages, field-of-view (FOV)=3.0x3.0 cm, slice thickness=0.5 mm, 20 slices, FA=90 deg, bandwidth (BW)=50 kHz, matrix=128x128, Total acquisition time= 6 m 25 s). Functional (BOLD) data were acquired using the same image geometry as the structural scans, with a two-shot, interleaved, gradient-echo echo planar imaging sequence with the following parameters: TE=15 ms, TR=1,500 ms (3,000 ms per volume), FA=70 degrees, BW 400 kHz and a data matrix of 128x64. 10 dummy scans were used to allow the T1 signal to reach steady-state prior to signal acquisition. After weighted Fourier transform to 128x128, the voxel resolution was 0.23x0.23x0.5 mm.

During functional imaging sessions, 10-cycles (30s on/30s off) of light stimulation (532 nm DPSS laser at 5-20 Hz, 50% duty cycle) were given to the cerebellum through an implanted optic fiber. Each 10-cycle epoch of stimulation was conducted as its own scan, and the laser pulse was driven by a TTL signal from a signal generator (Master-8) synced to the start of the imaging scan. We tested the effect of varied laser stimulus frequency (5, 10, 20 Hz) at intensities of 20 mW measured out of the 200 µm-diameter fiber terminus, corresponding to approximately 143 mW/mm^2 (Arch: n=5 mice; control: n=3 mice). On a separate set of mice, we tested power outputs of 5, 10, and 20 mW, which, at the 200 µm diameter fiber tip corresponded to spatial intensities of 10, 38, and 143 mW/mm^2, respectively (Arch: n=4 mice; control: n=4 mice). We imaged the frequency or intensity parameters (i.e. 5, 10, 20 Hz or 143, 38, 10 mW/mm^2) consecutively (i.e. 3 x 10 min) in a single scan, per mouse. At the brightest intensity (143 mW/mm^2) the luminance is predicted to drop to ~10% of maximum intensity within 600 µm of the face of the implanted fiber (https://web.stanford.edu/group/dlab/cgi-bin/graph/chart.php). Due to the laminar geometry and invaginations of the folia in the cerebellar cortex it is not straightforward to accurately predict the number of Purkinje neurons modulated in these experiments. However, we can estimate probable upper limits of the number of cells. For illumination of a sheet of densely packed Purkinje neurons (d.=30 µm), with circular illumination perpendicular to the plane of cells at a distance of 500 µm (25% max luminance; equates to a 420 µm circle) we calculate that ~200 Purkinje neurons would

likely be affected by the light stimulation. Alternatively, if the light was directed along the cross section of the folia, illuminating a trapezoidal array of Purkinje neurons with a height of 500 µm and bases of 200 (fiber diameter) and 420 µm (extent of luminance above 25% max) a total of ~220 Purkinje neurons would be affected by the light. Given these calculations, we predict that our stimulus effects on the order of up to a few hundred Purkinje neurons.

MRI analysis

Analysis was performed using FSL tools (see **Fig. S2** for an illustration of the analysis pipeline) (Smith et al., 2004). For each structural image, brain extraction was performed with BET (Smith, 2002) and signal inhomogeneity was corrected with FAST (Zhang et al., 2001). Motion correction of functional scans was performed with MCFLIRT, and slice timing was corrected. Scans with a large magnitude of head movement were identified and excluded from further analysis. Among the structural scans, a representative image was selected as the reference, to which all other structural images were registered using FLIRT. The same transformation matrix was then applied to functional (BOLD) scans. BOLD activation maps represented in **Figs. 2-4** were generated by statistical group comparisons of Arch>control.

Optimization of stimulation frequency and intensity: To compare the effect of various stimulation frequencies, statistically significant voxel activations in fMRI images were detected by first performing first-level FEAT (Woolrich, 2008) analysis ($p < 0.01$, $z > 3.1$; cluster-based thresholding, corrected for multiple comparisons), which uses univariate general linear modelling to fit voxel-wise data to a specified model, generating t values that are then transformed into standardized z values. For this study, we used a custom hemodynamic response (HR) model generated by averaging light-evoked BOLD signal time courses of all brain voxels using PEATE (**Fig. S3**, developed by Jonas T. Kaplan, http://www.jonaskaplan.com/peate/), then a higher-level FEAT analysis ($p < 0.001$, $z > 3.1$; cluster-based thresholding; corrected for multiple comparisons) between the Arch and control groups (**Fig. S2**). Comparison of varied stimulation intensity was performed using an identical pipeline, except that the higher-level analyses were performed at $p < 0.001$ and $z > 2.3$. For each stimulation parameter tested, the time course of BOLD activation in the motor cortex was exported by PEATE. The signal export was restricted only to significantly activated voxels in the 5 Hz group for the frequency dataset, and 143 mW/mm^2 group for the intensity dataset. F-tests were performed using higher-level FEAT analysis in FSL for a statistical comparison of group-level differences. Our design matrix consisted of 3 contrasts for both frequency and intensity comparisons (both 5, 10, or 20 Hz; and 143, 38, or 10 mW/mm^2). A significant difference was found between the intensity parameters ($p < 0.001$), but not frequency. We also performed additional Student's T-test comparisons of the pooled averages for each pairwise comparison (e.g. 5X10, 10X20, and 5X20 for frequency).

Identification of forebrain and midbrain regions modulated by cerebellar stimulation: All scans from Arch (n=9) and control (n=7) mice acquired with the 5 Hz, 143 mW/mm^2 stimulation parameter were combined from the frequency and intensity group for this analysis. Both first- and higher-level analyses were performed at the threshold of $p < 0.001$ and $z > 2.3$ using the cluster-based thresholding method in FEAT. Masks of brain structures were created by modifying an *in vivo* mouse brain atlas from the Computational Functional Anatomy Lab (National University of Singapore) and registering to the common space image. The number of activated voxels in each mask was quantified using the FSLstats command. The laterality index was calculated by subtracting the difference in the fraction of activated voxels (i.e. contralateral-ipsilateral) divided by the total fraction of activated voxels bilaterally. PEATE was used to construct activation time course graphs of all significantly activated voxels as well as for each brain mask (10 s baseline window, 50 s stimulus window).

Imaging and quantification of c-Fos expression post optogenetic stimulation

Optic fiber-implanted Arch and L7-cre control mice were optogenetically stimulated as described in the behavioral analysis section, but in a freely moving, home-cage setting. The stimulation parameters entailed 10-cycles (30s on/30s off) of laser stimulations (5 Hz, 50% duty cycle, ~143 mW/mm^2 intensity), as they were deemed optimal for inducing cerebellar output to the forebrain according to results from the ofMRI experiments. Post-stimulation, the mice were singly housed for 90 minutes, then deeply anesthetized with pentobarbital and intracardially perfused with 4% paraformaldehyde 0.1M phosphate-buffered saline (freshly diluted from 32% stock, Electron Microscopy Sciences). Brains were subsequently removed and incubated in 0.1M phosphate-buffered solution containing 30% sucrose at 4°C for up to 2 days. Brains were then embedded in optimal cutting temperature solution (TissueTech) at -80°C, and cryosectioned at 50 µm thickness.

Cerebellar sections were processed to confirm expression of the Arch opsin and fiber implantation. Cerebellar tissue sections were selected for immunostaining with rabbit polyclonal CaMKIIa antibody (1:300, LSBio) and goat anti-rabbit Alexa 568 secondary antibody (1:300). Tissue sections containing the motor and anterior cingulate cortices were selected for immunostaining with rabbit c-Fos polyclonal antibody (1:500, Santa Cruz) and goat anti-rabbit Alexa 568 secondary antibody (1:300, Life Technologies). Confocal images were obtained at 10, 20, and 63x magnification using a Zeiss 780 laser-scanning confocal microscope. At least 2 separate tissue sections from each mouse were imaged and analyzed using ImageJ (NIH). First, the images were thresholded to remove background signal. To establish counts, outlines over the motor and anterior cingulate cortices were drawn with references to The Allen Mouse Brain Atlas (Allen Institute, http://mouse.brain-map.org/) then the number of c-Fos positive cells was quantified using the "AnalyzeParticles" tool. Counts for each section were normalized to the size of selected area (Motor cortex: Arch, 1.10 ± 0.08 mm^2, n=4 mice; Ctrl, 1.34 ± 0.10 mm^2, n=4 mice; anterior cingulate cortex: Arch, 0.77 ± 0.05 mm^2, n=3 mice; Ctrl, 0.72 ± 0.05 mm^2, n=4 mice). Statistical comparisons were performed using Student's T-test with Prism 6 (Graphpad), where p-values less than 0.05 were considered to be statistically significant.

In vivo multi-electrode array recordings

A separate set of animals from those used in the ofMRI experiments were secured via a head bar to the recording apparatus and positioned on the top of a single axis rotating spherical Styrofoam ball. Animals were previously habituated to the entire apparatus over 2 consecutive days with at least 20 min. exposure per day. A 128 channel, 4-prong silicon based microprobe (Shobe et al., 2015) was inserted with stereotaxic guidance through the craniotomy and into the desired brain region to record the activity of multiple neurons simultaneously during optical manipulation of the forelimb region of the cerebellum. A TTL controlled (Master 8) 200 mW, 532 nm DPSS (OptoEngine) laser coupled to a fiber optic patch cable (Thorlabs) was connected to the horizontal optic cannula to generate laser pulses of various intensity and frequency during the recordings. The intensity of light output at the tip of the patch cable was calibrated at the start of every experiment and the intensity of light values reported is based on this intensity divided by the area of the fiber tip surface. Signals were recorded using an Intan amplifier evaluation system and USB interface (RHD2000) at a 25 kHz sampling rate. Recordings were made from the following brain regions (stereotaxic coordinates denote distance of tip of electrode from Bregma, in mm): motor cortex (X:1.0, Y:0, Z:1.2), retrosplenial cortex (X:0.5, Y:-1.5, Z:1.2), dorsal hippocampus (X:0.5, Y:-1.5, Z:2.4), and dorsal thalamus (X:0.5, Y:-1.5, Z:3.4). At the end of each recording, animals were intracardially perfused with 4% paraformaldehyde 0.1M phosphate-buffered solution (freshly diluted from 32% stock, Electron Microscopy Sciences) and the brains were fixed overnight prior to vibratome-sectioning at 100 μm thickness for post-hoc histological confirmation of fiber penetration site(s).

Semi-automated sorting of spike data was carried out offline using a template matching via stochastic batch optimization algorithm (Kilosort, https://github.com/cortex-lab/KiloSort) (Pachitariu et al., 2016). Sorted spikes were further clustered and attributed to single neuronal units using the Phy GUI (https://github.com/kwikteam/phy). We analyzed each data set across each of the different frequencies and intensities independently using the same parameter set for spike detection. Thus, cells represented across the horizontal in **Figs 2, 3C and 5B** are not the same. Data was further analyzed using custom Matlab routines (Shobe et al., 2015). Cells were determined to be modulated if at any time during the stimulus period their firing rate averaged over the 10 trials was determined to be excited, inhibited, or a mixture of both responses. Cells were deemed excited if their firing rate was 3 standard deviations above the baseline firing rate for 2 or more consecutive time bins. Cells were considered to be inhibited if either 1) their firing rate was 3 standard deviations below the baseline-firing rate for 2 or more consecutive time bins, or 2) their firing rate dropped to 0 Hz during the stimulus period for 5 or more consecutive time bins. Cells whose responses met the criteria for both excitation and inhibition at any time during the stimulus period were labelled as "mixed" units. No units displayed a decrease and then increase during the stimulus period. The baseline-firing rate was calculated as the average firing rate over the 10 second interval prior to stimulus onset. All spiking data was binned at 200 ms/bin. The mixed response units were excluded from the average unit plots in **Figs. 2, 3D, 5C** and **Fig. S7** due to the overall small proportion of cells displaying this type of activity and their high variability between cells. Peak and sustained responses were defined as the maximum spike response over the first 4 seconds and averaged spike response between 10 and 20 seconds after the onset of the light stimulation, respectively. All statistical comparisons of post spike sorted data were performed using Prism 6. Repeated measures (RM) ANOVA and post-hoc Tukey's multiple comparison tests for statistical analysis were conducted to compare the percentage of cells modulated across frequency and intensity. Kruskal-Wallis and post-hoc Dunn's multiple

comparison tests were conducted to test for statistical significance in the amplitude of peak and sustained firing rate responses. Outliers were identified using ROUT at Q=1% and removed from further analysis for **Figs. 2 and 3E and Fig. S7E**. All errors bars represent ± standard error of the mean.

RESULTS

Selective optogenetic activation of the forelimb region of the cerebellum

For this study, we chose to map regions of the forebrain and midbrain modulated by an area of the cerebellum associated with ipsilateral forelimb movement (Lee et al., 2015; Oscarsson and Uddenberg, 1964). We drove the output of this region in the cerebellar cortex, located between folia V and VI near the simplex lobule, using a previously employed optogenetic approach that can successfully drive motor output from discrete parts of a mouse's body (Lee et al., 2015). For this approach, we exploited a Cre-conditional mouse line (L7) to generate transgenic mice that selectively express the inhibitory opsin, archaerhodopsin-3 (Arch) fused to a green fluorescent protein (GFP), in Purkinje neurons (**Fig. 1A**). By activating Arch in a discrete subset of Purkinje neurons, we were able to selectively disinhibit a small population of neurons in the cerebellar nuclei that are involved in forelimb motor control (see **Fig. 1B** for schematic). To enable delivery of light to this region while performing a whole-brain fMRI scan, stereotaxic implantation of an optic fiber cannula was made at a horizontal angle rather than the conventional vertical angle (**Fig. 1C**). This approach allowed us to mount a four-channel radio-frequency receiver coil directly on top of an agar bridge-covered skull, thus improving signal-to-noise by optimal positioning of the coil and the agar bridge close to the brain. The direct abutment of the receiver coil to the head with the agar bridge significantly reduced imaging artifacts that can arise at transitions from air-filled spaces to animal tissue (Adamczak et al., 2010).

The fiber implantation site was easily identified within structural MR images, as well as in fixed brain tissue sections removed from mice at the end of experimentation (**Fig. 1D**). To further confirm proper stereotaxic positioning of the optic fiber, the fiber-implanted mice were tested for light-evoked forelimb movements in head-fixed, awake, behavioral assays. In a subset of these animals, we quantified their forelimb movement by combining high-speed videography and motion tracking enabled by placement of an infrared-reflective dot on the forelimb (**Fig. S4A**). Similar to our previous observation (Lee et al., 2015), light stimulation at 5 Hz (50% duty cycle) at an estimated intensity of 143 mW/mm^2 (20 mW output at the optical fiber tip) triggered short-latency upward movements of the ipsilateral forelimb in all of the tested Arch mice (n=4) (**Fig. S4**). The stereotyped movements were characterized by an initial fast retraction of the forelimb up and towards the body that begins at 20 ± 0 ms from light onset and lasts for 21 ± 4 ms (n=4). This initial movement was often followed by 1-3 smaller retracted movements that continued through to the end of the light stimulus. This response appeared qualitatively similar to defensive postural movements and those seen with stimulation of parts of the motor cortex (Hira et al., 2015). Furthermore, during a 5 Hz train of light stimuli the movements faithfully followed the stimulation periods (**Fig. S4B**). As demonstrated previously (Lee et al., 2015), fiber-implanted control mice, lacking expression of Arch, did not display light-induced forelimb movements (n=2 mice), negating the possibility that, with the stimulation parameters used for this study, laser-mediated heat production at the stimulation site in tissue lacking opsin expression can induce the observed movements (Stujenske et al., 2014).

Effects of stimulation frequency and intensity on forebrain activity

We sought to define an appropriate range of stimulation frequencies to induce fMRI-sensitive increases in forebrain BOLD signal triggered by optogenetic inhibition of cerebellar Purkinje neurons. Brain-wide BOLD signals were acquired from dexmedetomidine-sedated, head-fixed mice. During each 10-minute scanning session, light stimulation (532 nm wavelength) was delivered in a boxcar design through the implanted fiber. The pattern of stimulation consisted of 10-cycles of 30 s laser-pulse trains at 50% duty cycle, that is, 100 ms pulses at 5 Hz; 50 ms pulses at 10 Hz; or 25 ms pulses at 20 Hz with 30 s periods of laser off between each laser pulse cycle. We then analyzed the BOLD data using a custom model that was constructed by averaging brain-wide changes in the BOLD response (**Fig. S3**). Light stimulation at 5 Hz (50% duty cycle), 143 mW/mm^2 (20 mW output at the optical fiber tip) intensity induced a statistically significant increase in BOLD signal in motor-related forebrain structures such as the thalamus and motor cortex in Arch versus control mice (Arch (n=5)>control (n=3), p<0.001, z>2.3, cluster-corrected; **Fig. 2A,B; Fig. S5**). 48 (208 voxels) and 22 (58 voxels) percent of the total volume of the thalamus (433 voxels) and motor cortex (258 voxels) were contralaterally activated by these stimulation parameters. These significantly activated voxels were computed by a direct

comparison of changes in BOLD signal between Arch and control mice, precluding potentially significant effects arising from laser simulation artifacts such as tissue heating and light activation of the visual pathways (Schmid et al., 2016). In contrast to 5 Hz stimulation, we observed no significant differences (p>0.001, z<3.1) in BOLD signal in the motor cortex of Arch vs. control mice subjected to 10 (n=5 vs. 3, 0 activated voxels) or 20 Hz (n=4 vs. 3, 0 activated voxels) stimulation at the same light intensity. To further investigate the intensity and temporal dynamics of light stimulation-elicited BOLD response at these various stimulation frequencies, and to identify between-animal variability, the average time course of the motor cortex BOLD response was plotted. The baseline BOLD signal was stable across all animals tested, with only small fluctuations observed (**Fig. 2B**). Shortly after the 5 Hz stimulation onset, a peak increase in BOLD signal was observed, followed by a sustained increase throughout the stimulation period. Even though there was a small, but detectable transient change in BOLD signal, sustained responses during the stimulus period were not found during 10 and 20 Hz stimulation.

To assess the relationship between the BOLD signals and actual neural activity in the motor cortex, we examined the neural responses of the motor cortex to the same 5, 10, and 20 Hz optogenetic stimulation with *in vivo* electrophysiology in head restrained, un-anesthetized mice. Using a 128-channel silicon based multiprobe array we recorded single-cell and spike-time resolution action potential firing rates of motor cortex neurons while simultaneously modulating the forelimb region of the cerebellum via light stimulation. Across all frequencies, recorded cells in the motor cortex displayed a variety of responses to light induced cerebellar output (**Fig. 2C, D**; n=3 mice). The majority of cells that were significantly modulated (see methods) by light stimulation responded with an increase in firing rate within the stimulus period. The remaining fraction of modulated cells displayed either a decrease in firing rate or a mixture of both increased and decreased firing rates (see methods). Between the different frequencies of light stimulation we found a statistical difference in the percentage of cells modulated by the stimulus (Repeated measures ANOVA F(2,4)=14.65, p=0.01; **Fig. 2B left, Table 1**). At the 5 Hz stimulation frequency, we found the vast majority (90 ± 2%) of all recorded cells were modulated (i.e. excited, inhibited, or mixed) by the stimulus (**Fig. 2E, Table 1**). In contrast, stimulation at the higher frequencies (10 & 20 Hz) resulted in a significantly smaller percentage of cells being modulated (10 Hz: 43 ± 7%, 20, Hz: 50 ± 6%; **Fig. 2E, Table 1A**). At the population level, we found that the initial burst in firing rate of the excited cells (quantified as fold increase over baseline spiking frequency) displayed a small, but statistically significant difference across the 3 frequencies (Kruskal-Wallis test $\chi^2(3) = 6.794$, p=0.03; **Fig. 2D,E, Table 1B**). In comparison, we found a large difference in the neuronal firing rate during the sustained period following the initial burst in activity across the 3 examined frequencies (Kruskal-Wallis test $\chi^2(3) = 37.51$, p<0.0001; **Fig. 2E, Table 1C**), in close agreement with the characteristics of the BOLD time courses (**Fig. 2B**). No change in action potential firing rate was observed in response to light stimulation in control animals that lack expression of Arch opsin (**Fig. S6**). Although no statistical differences were found between the three frequencies in the ofMRI experiments (F-test, FSL FEAT, p>0.001), 5 Hz was deemed as the most suitable stimulation frequency for this study, since as detailed above, it (i) generated the highest number of activated voxels in the ofMRI dataset (**Fig. 2A**); and (ii) modulated a significantly higher percentage of cells and induced the largest sustained response in the electrophysiological dataset (**Fig. 2E**).

To determine whether the frequency (5 Hz) or duration (100 ms) of the light pulses we used was a more significant factor in driving downstream activation, we compared the percent of cells modulated in the motor cortex for the following stimulus parameters: 5 Hz stimulation with a 25 ms pulse width (12.5% duty cycle), 5 Hz stimulation with a 100 ms pulse width (50% duty cycle), and 20 Hz stimulation at a 25 ms pulse width (50% duty cycle). There was a significant effect on the percent of cells activated across all stimulus parameters (Repeated measures ANOVA F(2,4)=37.75, p=0.003; **Fig. S7**). We found that the shorter, 25 ms duration light pulse at 5 Hz modulated a significantly smaller percentage (16 ± 8%) of neurons in the motor cortex compared to the 100 ms duration stimulation at the same frequency (90%± 2%; Tukey's test p=0.002, n=3; **Fig. S7C**). Interestingly, the fraction of modulated neurons at 25 ms, 5 Hz stimulation was also significantly lower than that at 25 ms, 20 Hz stimulation (0.51 ± 0.06, Tukey's test p=0.03, n=3). In addition, the 25 ms duration light pulse resulted in a smaller sustained increase in firing rate as compared to the response to the 100 ms light pulse (0.6 ± 0.2 *vs.* 1.9 ± 0.2 fold increase over baseline, respectively; Dunn's test p=0.006, n=3 mice). These results indicate that the duration of the light pulse used to optogenetically modulate the cerebellar cortex has a significant impact on the effectiveness of this approach to drive cerebellar output.

To determine whether lower intensity light stimuli could be used to generate a similar response we next investigated the effect of varying light intensity while utilizing the 5 Hz frequency we found to best modulate the motor cortex in a separate group of mice. As illustrated in **Fig. 3A,B** and **Fig. S5B**, increasing the light intensity activated increasing numbers of voxels, and induced a stronger average BOLD signal in the motor cortex as well as the thalamus. At our lowest laser intensity, 10 mW/mm^2 we observed no statistically significant voxel activation in the motor cortex or thalamus and a small HR in both areas (**Fig. 3B, Fig. S5B left**; n=4). At the intermediate intensity of 38 mW/mm^2, we observed a few activated voxels (5/452 total) in the thalamus but not the motor cortex and a minor change in BOLD signal in both areas (**Fig. 3B, Fig. S5B middle**; n=4). Finally, laser stimulation at 143 mW/mm^2 resulted in significant activation of the motor cortex as well as an increased BOLD response, both of which were significantly greater compared to the 10 and 38 mW/mm^2 stimulation (two-tailed T-test, p<0.001; n=4 mice/group).

We again compared the neural spiking responses across these stimulation parameters, this time comparing the effects of intensity using *in vivo* electrophysiology (**Fig. 3C-E**). In agreement with our ofMRI data, we found that the stimulation intensities of 10 and 38 mW/mm^2 were not as effective as 143 mW/mm^2 at activating the motor cortex region. At these lower intensities, we found a much smaller percentage of cells modulated (excited, inhibited, or mixed) at 10 mW/mm^2 (30 ± 10%) and 38 mW/mm^2 (20 ± 8%) compared to the 143 mW/mm^2 stimulation (90 ± 2%; repeated measures ANOVA F(2,4)=45.2, p=0.0018; n=3 animals; **Fig. 3E left, Table 1**). Regarding the magnitude of the spike response, significant differences between the various intensities were found in both peak (Kruskal-Wallis test $\chi^2(3)$ = 6.794, p=0.03; **Fig 3E, middle**) and sustained responses (Kruskal-Wallis test $\chi^2(3)$ = 37.51, p<0.0001; **Fig. 3E, right**). Although we observed a large initial peak increase in firing rate at the 38 mW/mm^2 intensity, we did not find a comparable response in the ofMRI HR (**Fig. 3B**). It is likely that although the response in these cells is robust, the small percentage of cells excited (11 ± 5%, **Table 1**) does not produce enough of a metabolic load to significantly change the BOLD signal. Moreover, the necessary use of dexmedetomidine sedative, an α-2 adrenergic receptor inhibitor (Gertler et al., 2001), in the ofMRI experiments may additionally suppress changes in BOLD activity below a detectable level.

These combined ofMRI and *in vivo* electrophysiology data show that laser stimulation at the forelimb region of the lobulus simplex of Arch mice induces significant brain activation in motor-related regions of the forebrain consisting of the cerebello-thalamo-cortical pathway and feedback pathways from the forelimb, and that for the parameters we tested an intensity of 143 mW/mm^2 delivered at 5 Hz with a 50% duty cycle produces robust activation of these circuits. It should be noted that light intensity within the tissue drops to ~10% of maximum luminance within 600 μm of the optic fiber, thus the extent of light activation of Arch is relatively restricted to what is likely only a few 100 Purkinje neurons (see methods for calculation) located near the fiber (Huber et al., 2008).

Functional mapping of cerebellar cortical output targeting specific forebrain and midbrain regions

Combining the results from both the frequency and intensity data sets obtained at 5 Hz, 143 mW/mm^2, we conducted a brain-wide quantification of activated voxels within brain regions-of-interest (ROIs) defined by a parcellated anatomical atlas (**Fig. S8**) in order to identify the forebrain regions that become activated in response to optogenetic stimulation of the forelimb region of the cerebellum (**Fig. 4**). No statistical differences were found between these two datasets, collected from two different cohorts of mice (t-test, FSL FEAT, p>0.001). Light stimulation generated a discrete pattern of BOLD signal, with significantly activated voxels across a variety of forebrain and midbrain regions in Arch (n=9) versus control mice (n=7; p<0.001; **Fig. 4**, **Table 2**). Outside of motor areas like the thalamus and motor cortex, we also observed activation in putative non-motor forebrain regions involved in brain functions like cognition (e.g. infralimbic and anterior cingulate cortices), memory (e.g. hippocampus and retrosplenial cortex), and emotion (e.g. septal nuclei). Interestingly, when analyzed by individual brain region ROIs, we observed that different regions of the brain display HR waveforms of different shapes (compare **Fig. 5A** to whole brain **Fig. S9**). **Table 2** summarizes the absolute number of activated voxels per brain region and the percentage of activated voxels within each region.

To further support that the significant changes in BOLD signal we observed in multiple brain regions were related to changes in neural activity, we recorded the spiking activity of neurons in 4 brain regions that were significantly modulated during the ofMRI experiments. In addition to the motor cortex as detailed above, we recorded from the retrosplenial cortex, dorsal hippocampus, and dorsal thalamus due to our interest in these

regions and the fact that we could record serially from each of these regions at different depths in a single preparation. In all 4 regions, we found that a majority of neurons display significant changes in neural activity in response to cerebellar output (**Fig. 5B**). The dorsal thalamus displayed a large proportion of cells responding with a sustained increase (38%) or decrease (10%) throughout the stimulus in response to cerebellar output (36 modulated cells/ 69 total recorded cells). These sustained changes likely represent direct input from the cerebellum, and support our prior findings that disinhibition of cerebellar nuclear neurons results in sustained bursts of activity capable of driving activation in downstream sites (Lee et al., 2015). Only 3 cells responded with a mixture of excitation and inhibition during the stimulus period.

In the dorsal hippocampus 70% of cells responded to the stimulus (41/59 total recorded). The excited cells (18, 44% of all modulated cells) responded mostly with a transient response, with a bursting at either the onset (15%), offset (3%), or both periods (14%) (**Fig. 5B**). 15% of all cells showed activation throughout the majority of the stimulus period, while 24% showed inhibited firing rates. In the retrosplenial cortex, we found a mixture of responses to stimulation with 74% of all cells modulated by cerebellar output (52/70 cells total) (**Fig. 5B**). In the 51% of cells that were excited, many responded only during the first ~15 s of the stimulus, while others responded late in the pulse sequence. In 9% of all cells in the retrosplenial cortex, the excitatory component was followed by a significant decrease in firing rate below baseline. We also observed a number of neurons that were significantly suppressed/inhibited during the stimulus (11% of all cells).

To confirm cellular activation in the motor and anterior cingulate cortex triggered by optogenetic stimulation of the cerebellar forelimb region, we quantified the number of neurons expressing c-Fos, a widely-used histological marker that labels neurons that have undergone increased activity (Sagar et al., 1988). Light stimulation (143 mW/mm^2, 5 Hz for 10 minutes) led to a significantly higher number of c-Fos positive cells in both regions in Arch mice when compared to controls (motor cortex: Arch, 104.1 ± 21.3 per mm^2, n=4 mice vs. control, 25.3 ± 9.8 per mm^2, n=4 mice, p=0.015; anterior cingulate cortex: Arch, 92.6 ± 8.3 per mm^2, n=3 mice vs. control, 41.8 ± 12.2 per mm^2, n=4 mice, p=0.025; unpaired, two-tailed t-test, **Fig. 6**). These results support the validity of our method for detecting forebrain and midbrain regions activated by optogenetic stimulation of cerebellar cortex using BOLD signal as a readout. Additionally, these results demonstrate the functional relevance of synaptic connections between the forelimb region of the cerebellar cortex and primary motor cortex, previously mapped with trans-synaptic tract tracing methods (Kelly and Strick, 2003).

DISCUSSION

Although computations at the regional circuit level are critical for controlling certain aspects of behavior, complex behavioral output is ultimately produced by interactions between brain regions. Results from prior experiments have hinted that the cerebellum is highly interconnected, in many cases via the thalamus, with several regions of the forebrain and midbrain including the striatum, motor cortex, prefrontal cortex and ventral tegmental area (Clower et al., 2001; Hoover and Strick, 1999; Kelly and Strick, 2003; Lin et al., 2014; Lynch et al., 1994; Middleton and Strick, 2001). However, most of these studies have examined forebrain and midbrain projections originating from the cerebellar nuclei rather than the cerebellar cortex, considered the computational center of the cerebellum. Here we describe a method with which to define functional connections between discrete regions of the cerebellar cortex and the forebrain using a combined optogenetic and fMRI method, overcoming the challenges of classical methods used for identifying functionally or anatomically connected brain regions. Using a known cerebellum-to-forebrain pathway, we first defined a set of optogenetic stimulation parameters capable of generating reliable but specific forebrain BOLD and electrophysiological responses (**Fig. 1-3**). We then identified a set of forebrain and midbrain regions that are functionally activated by pausing Purkinje neurons in a forelimb region of the cerebellar cortical area between folia V and VI near the simplex lobule. We observed that optogenetic stimulation of this region causes robust activation in the thalamus and motor cortex, expected results given the area's implication in forelimb movement (Casabona et al., 2003; Ekerot et al., 1997; Kelly and Strick, 2003; Lee et al., 2015); we also found that this region of cerebellum can alter, directly or indirectly, neural activity in putative non-motor areas such as the hippocampus and anterior cingulate cortex **(Fig. 4-6)**.

Across the parameters tested, 5 Hz stimulation at a 50% duty cycle and 143 mW/mm^2 intensity produced the most reliable downstream changes in BOLD signal and electrophysiological activity in forebrain and midbrain areas. A few possibilities exist as to why we found that lower intensities and shorter stimulus pulse

durations are less effective at generating cerebellar output. First, the lower BOLD responses resulting from the low intensity, or high frequency stimulations may in part be due to lingering effects of the prior stimulus epoch, as our scans were performed with a decreasing order of intensities (i.e. 143, 38, 10 mW/mm^2) and increasing order of frequency (i.e. 20, 10, 5 Hz). However, we found no cycle-to-cycle decrease in the response to stimulation (**SFig. 3**), indicating that there is no long-lasting effect on the circuits modulated. Second, although optogenetic inhibition of Purkinje neuron firing can be generated reliably with light pulses as short as 10 ms (Lee et al., 2015), Purkinje neuron pauses of this duration may fail to induce excitation of the downstream cerebellar nuclear neurons. Even though single-pulse, transient suppression of Purkinje axonal spiking activity as brief as 25 ms can generate bursts of action potential firing in cerebellar nuclear neurons *in vivo* (Lee et al., 2015), this may not be the case for optogenetic suppression of spiking at the soma and dendrite and/or over multiple pulses as performed in experiments detailed here. Another possibility is that pulse durations under 100 ms are unable to bring a large enough population of Purkinje neurons to pause significantly prior to the end of each pulse, preventing significant output toward the forebrain. This may be especially true for Purkinje neurons more distant to the site of fiber optic stimulation that receive significantly lower intensities of light, and therefore require additional time to reach a suppressed state. Overall, we find that longer pulses and lower frequency stimulation best drive downstream activation that can be assessed using our ofMRI approach, findings that are consistent with other studies examining cerebellar forebrain connectivity (Parker et al., 2017).

We found that forebrain HR generated by optogenetic stimulation of the cerebellar cortex had a multimodal waveform over the course of the ten-minute stimulus that appears to be related to changes in neuronal firing rate. For 5 Hz, 143 mW/mm^2 stimuli, we observed that both the HR and neural firing rate in the motor cortex responded to the stimulus with an initial peak increase, followed by a sustained response. At higher frequency stimulation, the sustained increase was absent, both in the HR and recorded neural activity. These corresponding changes in the HR and neural firing rate reinforce the notion that the changes in BOLD signals we recorded are well correlated to changes in neural activity, although with slower temporal dynamics. Our data suggest that the BOLD changes we observed are related mostly to the excitation, rather than inhibition of neurons, as the average responses of the inhibited neurons did not appear to match that of the HR during the 5 Hz, 143 mW/mm^2 stimulation. These results are in line with prior findings (Waldvogel et al., 2000). One technical challenge not easily overcome for regions of the cerebellum where stimulation results in motor behavioral output (i.e. limb movement), are indirect effects due to sensory or proprioceptive input related to forelimb movement. However, we believe that the reduced movement of the forelimb produced under sedation and the relatively limited extent of activation in the somatosensory cortex we observed (~4.5% of all voxels in the region), indicates that it contributes to only a part of the detected BOLD signals we report.

We find that optogenetic stimulation of the forelimb region of the cerebellar cortex, located near lobule V-VI just lateral to the vermis, leads to BOLD activation, modulated neuronal activity, and an increased number of c-Fos positive cells in the primary motor cortex (**Fig. 2-3, 6**). These results demonstrate the existence of functional pathways through which this cerebellar region can influence forebrain motor regions, in accordance with results from trans-synaptic tract tracing methods in Cebus monkeys (Kelly and Strick, 2003). This serves as strong proof-of-principle evidence for the robustness of the ofMRI method we describe here, since the existence of interactions between the cerebellum and motor cortex is well established (Allen and Tsukahara, 1974; Daskalakis et al., 2004; Massion and Rispal-Padel, 1972; Proville et al., 2014; Thach, 1975). How these two major motor areas work in conjunction during motor behavior and learning is not fully understood (Galea et al., 2011; Kishore et al., 2014; Proville et al., 2014). The ofMRI method may be suitable for answering specific questions; for example, by using longitudinal connectivity mapping at different stages of optogenetically-induced associative motor learning to visualize how the connectivity relationship between these two brain areas evolves over time.

In addition to the motor cortex, we find significant increases in BOLD signal in a number of other regions including the hippocampus (**Fig. 4-5**; See **Table 2** for full list). The hippocampus is known to play a critical role in spatial learning and memory, and deficits in its function disrupt cerebellar-mediated behaviors like trace eye-blink conditioning (McGlinchey-Berroth et al., 1997; Solomon et al., 1986; Weiss et al., 1999; Yu and Krook-Magnuson, 2015). Previous reports indicate that direct connections between the cerebellum and hippocampus may exist (Arrigo et al., 2014; Liu et al., 2012), and there is highly suggestive data that interactions between the two regions are involved in animal behaviors such as pattern separation and temporal aspects of spatial movement and navigation (Burguiere et al., 2005; Paleja et al., 2014; Rochefort et al., 2011). Additionally,

direct stimulation of the cerebellum evokes action potentials in the hippocampus and can suppress hippocampal seizures (Krook-Magnuson et al., 2014; Newman and Reza, 1979). Our data further corroborates these prior findings and indicates that the forelimb region of the cerebellum interacts with the dorsal hippocampus. While we do not yet know the specifics of the connectivity between the two regions, a potential relay may occur by way of the septal nuclei (Heath et al., 1978), which we also find significantly activated by our stimulation. Future experiments utilizing retrograde trans-synaptic tracers injected in the dorsal hippocampus would likely provide clearer understanding of how these brain regions are connected and further *in vivo* recordings would help to elucidate the dynamics of this functional connection.

We also found significant changes in BOLD signal in the anterior cingulate and retrosplenial cortices (**Fig. 4-5**), results we validated with *in vivo* electrophysiology for both regions (**Fig. 5**) and histology for the former region (**Fig. 6**). These two regions are implicated in a variety of behaviors including episodic memory, impulse control, and emotion (Amianto et al., 2013). Interestingly, prior studies suggest the anterior cingulate cortex is activated during decisions that produce internal conflict resulting in increased errors in behavioral output (Botvinick et al., 1999; Braver et al., 2001; Bush et al., 2000). As the cerebellum is often described as a highly plastic circuit that makes learning-dependent neural changes triggered by unexpected events or errors in behavioral output, the role of connectivity with these regions may be to provide them with information about ongoing errors in motor and/or behavioral output (Ito, 2013; Ohmae and Medina, 2015; Ohyama et al., 2003). To the best of our knowledge, no direct methods (e.g. tract tracing or electrophysiological) have yet demonstrated the existence of cerebellar projections toward the anterior cingulate cortex in animals. And while it is possible that the activation we observe in this region is related to indirect effects, there are multiple, recent resting-state fMRI studies in humans that support our finding of a functional connection between these two regions (Amianto et al., 2013; Liu et al., 2010). Furthermore, significant parallel changes in the functional connectivity are observed between these two regions in patients with major depression and eating disorders (Amianto et al., 2013; Liu et al., 2010), signifying potential clinical relevance of the functional connectivity between these brain regions and thus prompting further investigation.

Unlike transneuronal viral tracing methods, which are predicated on injections into specific regions of the forebrain suspected to be connected to a given region of the cerebellar cortex based on *a priori* evidence, the ofMRI method allows one to observe activation of discrete brain regions within a single experiment across the whole brain. Another major advantage of this approach is the ability to monitor functional connectivity over time in multiple scans, allowing one to monitor changes related to learning, age, or disease processes. In various rodent models this approach is well suited to be used as a platform to examine how cerebellar-related diseases, like autism spectrum disorder, dystonia, and essential tremor disrupt interactions between the cerebellum and forebrain as well as how potential therapeutics may treat these disruptions.

Seminal work by Strick and others in the 1990s transformed views on cerebellum to forebrain connectivity (Dum and Strick, 2003; Hoover and Strick, 1999; Middleton and Strick, 1994; Mushiake and Strick, 1993). Up until that point, it was widely held that motor planning and cognitive-related neural information flowed in an open loop from forebrain regions to the cerebellum via the pontine nucleus, but not from the cerebellum back to those regions, with the exception of the cerebello-thalamic-motor cortex loop (Brodal and Hoddevik, 1978; Schmahmann and Pandya, 1997; Yeo et al., 1985). Using transneuronal tract tracing methods, Strick demonstrated that distinct regions of the cerebellum project back to the forebrain via the thalamus, thus indicating that the cerebellum-forebrain system is a closed rather than open system. The transformative implication of these findings was that the cerebellum is not subservient to higher order cognitive processing but may instead play a significant role in cognitive processing itself. Ideas surrounding the importance of the cerebellum in non-motor function were advanced by Schmahmann and colleagues who through clinical and experimental observation linked disruptions in cerebellar function with non-motor dysfunction (Schmahmann, 1996; Schmahmann, 2000; Schmahmann, 2004; Schmahmann and Sherman, 1997). More recent work by Buckner and colleagues suggested that the cerebellum and neocortex have widespread systematic connectivity (Buckner, 2013). Using ofMRI we demonstrate that the forelimb region of the cerebellar cortex influences a broad set of forebrain and midbrain regions thought to be involved in distinct aspects of behavior. These results add to the growing consensus that interactions between the cerebellum and various regions of the forebrain and midbrain are important in the execution of a broad array of behaviors.

ACKNOWLEDGEMENTS

FIGURE LEGENDS

Figure 1. Light activation of Arch in Purkinje neurons drives cerebellar output during fMRI scans. (A) Parasagittal cerebellar brain slice from an L7-Cre;RCL-Arch-GFP mouse showing selective Purkinje neuron expression of the Arch-GFP transgene (green). Arch-GFP expression is apparent in the membranes of Purkinje neuron soma and dendritic trees (**right**, **top**) as well as its axons (**right**, **bottom**) projecting to cerebellar nuclear neurons (blue, CamKIIa) **(B)** A schematic describing the use of inhibitory optogenetics to generate cerebellar output to the forebrain. At steady-state Arch expressing Purkinje neurons (green) tonically inhibit cerebellar nuclear neurons (black), thereby limiting cerebellar output to downstream sites like the forebrain. Synchronous pauses in discrete populations of Purkinje neurons during light activation of Arch disinhibits the cerebellar nucleus, thus driving cerebellar output. **(C)** Fiber optic cannulas were stereotaxically placed in the forelimb region of the cerebellar cortex at a 0^0 angle (horizontal) through a craniotomy in the caudal part of the occipital bone. **(D)** The implantation site is apparent in both exemplar histological section (**left**) and MRI structural scan (**right**) containing the cerebellum. The location of the implanted optic fiber (see red arrows) is visible as a dark area juxtaposed to the vermis near the medial simplex.

Figure 2. Lower frequency light pulses effectively drive neural activity in the motor cortex. (A) OfMRI BOLD signals (Arch>control) were imaged during 10 x 30 s long epochs of 5, 10, and 20 Hz light stimulation (50% duty cycle, 143 mW/mm^2 intensity) interleaved with 10 x 30 s long rest periods (no light pulse). An atlas of subdivided brain structures (black lines) is overlaid on top of the BOLD signal (yellow-red) and representative structural images (grayscale) at 2 different slice planes (Y: 0.26 and -2.7 from Bregma). White arrow points to motor cortex activation in the 5 Hz stimulation condition. **(B)** Time course of average percent change in BOLD activation for Arch (red, n=4-5 mice) and control (black, n=3 mice) animals stimulated at 5, 10, and 20 Hz, calculated in a subregion of the contralateral motor cortex containing significantly activated voxels in the 5 Hz Arch group (**A**, **left**). The light was pulsed during the time window indicated by the green bar. Shaded areas indicate s.e.m. **(C)** The fold change in baseline subtracted firing rate ((R-R0)/R0) is shown for all recorded motor cortical neurons during the 5 (n=107), 10 (n=159), and 20 (n=114) Hz stimulation period (green bar; n=3 animals). Responses are thresholded to 10x the fold rate change to improve visualization of neural activity. Starting from the top, every 50th cell is marked by a tick along the y-axis (i.e. y-axis=50 cells/tick). 200 ms/bin **(D)** The average neural response across cells that were significantly excited (red) and inhibited (purple) is plotted for each frequency. **(E) Left**, summary graph of the percent of cells modulated and the modulation type for each frequency of stimulation (one-way ANOVA with post-hoc Tukey's test *p<0.05). The average magnitude of the initial peak (0-4 ms, **middle**) and sustained increase (averaged between 10-20 ms, **right**) for all excited cells is plotted for each frequency (Kruskal-Wallis with post-hoc Dunn's test *p<0.05, ****p<0.0001).

Figure 3. Effects of light intensity on the modulation of neural activity in the motor cortex. (A) OfMRI BOLD signals (Arch>control) generated by 3 different light intensities applied at 5 Hz. As in **Fig. 2**, an atlas of subdivided brain structures (black lines) is overlaid on top of the BOLD signal (yellow-red) and representative structural images (grayscale) at 2 different slice planes (Y: -0.22 and -2.7 mm from Bregma). **(B)** Time course of average percent change in BOLD activation (red) and control (black) at each indicated intensity (n=4 mice/group), calculated in a subregion of the contralateral motor cortex containing significantly activated voxels in the 143 mW/mm^2 Arch group (**A**, **left**). The light was pulsed at 5 Hz during the time window indicated by the green bar. Shaded areas indicate s.e.m. **(C)** The fold change in baseline subtracted firing rate ((R-R0)/R0) is shown for all recorded cells during the, 10 (n=97), 38 (n=109), 143 (n=107) mW/mm^2 stimulation period (green bar; n=3 animals). Responses are thresholded to 10x the fold rate change to improve visualization of neural activity. Starting from the top, every 50th cell is marked by a tick along the y-axis (i.e. y-axis=50 cells/tick). 200 ms/bin **(D)** The average neural response across cells that were significantly excited (red) and inhibited (purple) is plotted for each frequency. **(E) Left**, summary graph of the percent of cells modulated and the modulation type for each frequency of stimulation (one-way ANOVA with post-hoc Tukey's test **p<0.01 The average magnitude of the initial peak (0-4 ms, **middle**) and sustained increase (averaged between 10-20 ms, **right**) for all excited cells is plotted for each frequency (Kruskal-Wallis with post-hoc Dunn's test *p<0.05, **p<0.01, ***p<0.001)

Figure 4. Cerebellar stimulation drives changes in BOLD signal in various forebrain and midbrain regions. (A) Changes in BOLD signal are overlaid onto MRI images taken at 0.5 mm intervals. Changes in

BOLD signal were induced by a 5 Hz, 100 ms long light train delivered to the cerebellar forelimb region. Significant changes in signal are averaged across the 10 alternating on and off cycles over a 10-minute period. Z-scores were calculated for statistically significant changes in BOLD signal in Arch (n=9) vs control (n=7) animals (p<0.001). Brain regions are labelled according to 3-D mouse brain atlas (**Fig. S9**). Images are organized from rostral to caudal. Infralimbic Cortex (ILC), Motor Cortex (MC), Anterior Cingulate Cortex (ACC), Septal Nuclei (SpN), Somatosensory Cortex (SSC), Hippocampus (Hpc), Thalamus (Th), Retrosplenial Cortex (RsC), Reticular Formation (RF), Entorhinal Cortex (EC), Periaqueductal Gray (PAG).

Figure 5. The cerebellar forelimb region can modulate activity of putative cells in the dorsal thalamus, retrosplenial cortex, dorsal hippocampus, and motor cortex. (A) Top, anatomical masks overlaid on an example coronal structural for the indicated brain region. **Bottom**, the average BOLD time course is plotted for the entire thalamus, retrosplenial cortex, hippocampus, and motor cortex (red: Arch, n=9; black: control, n=7). A 5 Hz, 143 mW/mm^2 stimulus was applied during the 30 s pulse indicated by the green bar. **(B)** To visualize and compare the temporal dynamics of the spiking response between activated brain regions, the change in firing rate from baseline is normalized to the max rate, unlike **Figs. 2,3C**. Only the cells found to be modulated in the four regions are displayed (dorsal thalamus n=36 modulated/69 total, retrosplenial cortex n=53/70, dorsal hippocampus n=41/59, and motor cortex n=107/120), y-axis = 15 cells/tick. **(C)** The average change in firing rate from baseline normalized to peak firing rate is displayed for the excited (red) and inhibited (purple) cells.

Figure 6. Light stimulation increases the number c-Fos+ cells in the motor and anterior cingulate cortices. (A) Confocal micrographs of c-Fos (red) and DAPI (grey) immunostained coronal brain sections from an Arch-expressing (left) and control (right) mouse. Light stimulation parameters at the forelimb region of the cerebellar cortex was identical to that of ofMRI scans (5 Hz, 143 mW/mm^2, 30 s alternating on and off for 10 minutes). A higher number of c-Fos+ cells are visible in the motor cortex (MC) and anterior cingulate cortex (ACC) of Arch mice compared to control. Thresholded c-Fos+ cells in the MC **(B)** and ACC **(C)** of Arch (top) and L7-cre control (middle) mice, detected by particle analysis. Scatter plots at the bottom represent normalized c-Fos+ cell count in each region of Arch and control mice (ACC located between dashed lines in **C**). Lines represent average ±SEM. * denotes p<0.05. SSC, somatosensory cortex; CC, corpus callosum. All scale bars represent 500 μm.

REFERENCES CITED

Adamaszek, M., D'Agata, F., Ferrucci, R., Habas, C., Keulen, S., Kirkby, K.C., Leggio, M., Marien, P., Molinari, M., Moulton, E., Orsi, L., Van Overwalle, F., Papadelis, C., Priori, A., Sacchetti, B., Schutter, D.J., Styliadis, C., Verhoeven, J., 2017. Consensus Paper: Cerebellum and Emotion. Cerebellum 16, 552-576. http://doi.org/10.1007/s12311-016-0815-8

Adamczak, J.M., Farr, T.D., Seehafer, J.U., Kalthoff, D., Hoehn, M., 2010. High field BOLD response to forepaw stimulation in the mouse. Neuroimage 51, 704-712. http://doi.org/10.1016/j.neuroimage.2010.02.083

Akkal, D., Dum, R.P., Strick, P.L., 2007. Supplementary motor area and presupplementary motor area: targets of basal ganglia and cerebellar output. J Neurosci 27, 10659-10673. http://doi.org/10.1523/jneurosci.3134-07.2007

Allen, G.I., Tsukahara, N., 1974. Cerebrocerebellar communication systems. Physiol Rev 54, 957-1006.

Amianto, F., D'Agata, F., Lavagnino, L., Caroppo, P., Abbate-Daga, G., Righi, D., Scarone, S., Bergui, M., Mortara, P., Fassino, S., 2013. Intrinsic Connectivity Networks Within Cerebellum and Beyond in Eating Disorders. The Cerebellum 12, 623-631. http://doi.org/10.1007/s12311-013-0471-1

Apps, R., Hawkes, R., 2009. Cerebellar cortical organization: a one-map hypothesis. Nat Rev Neurosci 10, 670-681. http://doi.org/10.1038/nrn2698

Arrigo, A., Mormina, E., Anastasi, G.P., Gaeta, M., Calamuneri, A., Quartarone, A., De Salvo, S., Bruschetta, D., Rizzo, G., Trimarchi, F., Milardi, D., 2014. Constrained spherical deconvolution analysis of the limbic network in human, with emphasis on a direct cerebello-limbic pathway. Front Hum Neurosci 8, 987. http://doi.org/10.3389/fnhum.2014.00987

Balsters, J.H., Laird, A.R., Fox, P.T., Eickhoff, S.B., 2014. Bridging the gap between functional and anatomical features of cortico-cerebellar circuits using meta-analytic connectivity modeling. Hum Brain Mapp 35, 3152-3169. http://doi.org/10.1002/hbm.22392

Bernal-Casas, D., Lee, H.J., Weitz, A.J., Lee, J.H., 2017. Studying Brain Circuit Function with Dynamic Causal Modeling for Optogenetic fMRI. Neuron 93, 522-532.e525. http://doi.org/10.1016/j.neuron.2016.12.035

Bernard, J.A., Seidler, R.D., Hassevoort, K.M., Benson, B.L., Welsh, R.C., Wiggins, J.L., Jaeggi, S.M., Buschkuehl, M., Monk, C.S., Jonides, J., Peltier, S.J., 2012. Resting state cortico-cerebellar functional connectivity networks: a comparison of anatomical and self-organizing map approaches. Frontiers in Neuroanatomy 6, 31. http://doi.org/10.3389/fnana.2012.00031

Bostan, A.C., Dum, R.P., Strick, P.L., 2013. Cerebellar networks with the cerebral cortex and basal ganglia. Trends Cogn Sci 17, 241-254. http://doi.org/10.1016/j.tics.2013.03.003

Botvinick, M., Nystrom, L.E., Fissell, K., Carter, C.S., Cohen, J.D., 1999. Conflict monitoring versus selection-for-action in anterior cingulate cortex. Nature 402, 179-181. http://doi.org/10.1038/46035

Braver, T.S., Barch, D.M., Gray, J.R., Molfese, D.L., Snyder, A., 2001. Anterior Cingulate Cortex and Response Conflict: Effects of Frequency, Inhibition and Errors. Cerebral Cortex 11, 825-836. http://doi.org/10.1093/cercor/11.9.825

Brodal, A., Hoddevik, G.H., 1978. The pontocerebellar projection of the uvula in the cat. Exp Brain Res 32, 105-116. http://doi.org/10.1007/BF00237395

Buckner, R.L., 2013. The cerebellum and cognitive function: 25 years of insight from anatomy and neuroimaging. Neuron 80, 807-815. http://doi.org/10.1016/j.neuron.2013.10.044

Buckner, R.L., Krienen, F.M., Castellanos, A., Diaz, J.C., Yeo, B.T., 2011. The organization of the human cerebellum estimated by intrinsic functional connectivity. J Neurophysiol 106, 2322-2345. http://doi.org/10.1152/jn.00339.2011

Burguiere, E., Arleo, A., Hojjati, M., Elgersma, Y., De Zeeuw, C.I., Berthoz, A., Rondi-Reig, L., 2005. Spatial navigation impairment in mice lacking cerebellar LTD: a motor adaptation deficit? Nat Neurosci 8, 1292-1294. http://doi.org/10.1038/nn1532

Bush, G., Luu, P., Posner, M.I., 2000. Cognitive and emotional influences in anterior cingulate cortex. Trends Cogn Sci 4, 215-222. http://doi.org/10.1016/S1364-6613(00)01483-2

Casabona, A., Valle, M.S., Bosco, G., Garifoli, A., Lombardo, S.A., Perciavalle, V., 2003. Anisotropic representation of forelimb position in the cerebellar cortex and nucleus interpositus of the rat. Brain Res 972, 127-136. http://doi.org/10.1016/S0006-8993(03)02513-7

Chan, R.W., Leong, A.T.L., Ho, L.C., Gao, P.P., Wong, E.C., Dong, C.M., Wang, X., He, J., Chan, Y.S., Lim, L.W., Wu, E.X., 2017. Low-frequency hippocampal-cortical activity drives brain-wide resting-state functional MRI connectivity. Proc Natl Acad Sci U S A 114, E6972-E6981. http://doi.org/10.1073/pnas.1703309114

Chen, C.H., Fremont, R., Arteaga-Bracho, E.E., Khodakhah, K., 2014. Short latency cerebellar modulation of the basal ganglia. Nat Neurosci 17, 1767-1775. http://doi.org/10.1038/nn.3868

Clower, D.M., West, R.A., Lynch, J.C., Strick, P.L., 2001. The inferior parietal lobule is the target of output from the superior colliculus, hippocampus, and cerebellum. J Neurosci 21, 6283-6291.

Crippa, A., Del Vecchio, G., Busti Ceccarelli, S., Nobile, M., Arrigoni, F., Brambilla, P., 2016. Cortico-Cerebellar Connectivity in Autism Spectrum Disorder: What Do We Know So Far? Frontiers in Psychiatry 7, 20. http://doi.org/10.3389/fpsyt.2016.00020

Daskalakis, Z.J., Paradiso, G.O., Christensen, B.K., Fitzgerald, P.B., Gunraj, C., Chen, R., 2004. Exploring the connectivity between the cerebellum and motor cortex in humans. J Physiol 557, 689-700. http://doi.org/10.1113/jphysiol.2003.059808

Dum, R.P., Strick, P.L., 2003. An unfolded map of the cerebellar dentate nucleus and its projections to the cerebral cortex. J Neurophysiol 89, 634-639. http://doi.org/10.1152/jn.00626.2002

Ekerot, C.F., Garwicz, M., Jorntell, H., 1997. The control of forelimb movements by intermediate cerebellum. Prog Brain Res 114, 423-429. http://doi.org/10.1016/S0079-6123(08)63378-6

Ferenczi, E.A., Zalocusky, K.A., Liston, C., Grosenick, L., Warden, M.R., Amatya, D., Katovich, K., Mehta, H., Patenaude, B., Ramakrishnan, C., Kalanithi, P., Etkin, A., Knutson, B., Glover, G.H., Deisseroth, K., 2016. Prefrontal cortical regulation of brainwide circuit dynamics and reward-related behavior. Science 351, aac9698. http://doi.org/10.1126/science.aac9698

Galea, J.M., Vazquez, A., Pasricha, N., de Xivry, J.J., Celnik, P., 2011. Dissociating the roles of the cerebellum and motor cortex during adaptive learning: the motor cortex retains what the cerebellum learns. Cereb Cortex 21, 1761-1770. http://doi.org/10.1093/cercor/bhq246

Gertler, R., Brown, H.C., Mitchell, D.H., Silvius, E.N., 2001. Dexmedetomidine: a novel sedative-analgesic agent. Proceedings (Baylor University. Medical Center) 14, 13-21. http://doi.org/10.1590/S0034-70942012000100015

Grodd, W., Hulsmann, E., Lotze, M., Wildgruber, D., Erb, M., 2001. Sensorimotor mapping of the human cerebellum: fMRI evidence of somatotopic organization. Hum Brain Mapp 13, 55-73. http://doi.org/10.1002/hbm.1025/pdf

Halko, M.A., Farzan, F., Eldaief, M.C., Schmahmann, J.D., Pascual-Leone, A., 2014. Intermittent theta-burst stimulation of the lateral cerebellum increases functional connectivity of the default network. J Neurosci 34, 12049-12056. http://doi.org/10.1523/JNEUROSCI.1776-14.2014

Han, V.Z., Magnus, G., Zhang, Y., Wei, A.D., Turner, E.E., 2014. Bidirectional modulation of deep cerebellar nuclear cells revealed by optogenetic manipulation of inhibitory inputs from Purkinje cells. Neuroscience 277, 250-266. http://doi.org/10.1016/j.neuroscience.2014.07.006

Heath, R.G., Dempesy, C.W., Fontana, C.J., Myers, W.A., 1978. Cerebellar stimulation: effects on septal region, hippocampus, and amygdala of cats and rats. Biol Psychiatry 13, 501-529.

Heiney, S.A., Kim, J., Augustine, G.J., Medina, J.F., 2014. Precise control of movement kinematics by optogenetic inhibition of Purkinje cell activity. J Neurosci 34, 2321-2330. http://doi.org/10.1523/jneurosci.4547-13.2014

Hira, R., Terada, S., Kondo, M., Matsuzaki, M., 2015. Distinct Functional Modules for Discrete and Rhythmic Forelimb Movements in the Mouse Motor Cortex. J Neurosci 35, 13311-13322. http://doi.org/10.1523/jneurosci.2731-15.2015

Hoover, J.E., Strick, P.L., 1999. The organization of cerebellar and basal ganglia outputs to primary motor cortex as revealed by retrograde transneuronal transport of herpes simplex virus type 1. J Neurosci 19, 1446-1463.

Huang, C.C., Sugino, K., Shima, Y., Guo, C., Bai, S., Mensh, B.D., Nelson, S.B., Hantman, A.W., 2013. Convergence of pontine and proprioceptive streams onto multimodal cerebellar granule cells. Elife 2, e00400. http://doi.org/10.7554/eLife.00400

Huber, D., Petreanu, L., Ghitani, N., Ranade, S., Hromadka, T., Mainen, Z., Svoboda, K., 2008. Sparse optical microstimulation in barrel cortex drives learned behaviour in freely moving mice. Nature 451, 61-64. http://doi.org/10.1038/nature06445

Ichinohe, N., Mori, F., Shoumura, K., 2000. A di-synaptic projection from the lateral cerebellar nucleus to the laterodorsal part of the striatum via the central lateral nucleus of the thalamus in the rat. Brain Res 880, 191-197. http://doi.org/10.1016/S0006-8993(00)02744-X

Ito, M., 2013. Error detection and representation in the olivo-cerebellar system. Front Neural Circuits 7, 1. http://doi.org/10.3389/fncir.2013.00001

Kelly, R.M., Strick, P.L., 2003. Cerebellar loops with motor cortex and prefrontal cortex of a nonhuman primate. J Neurosci 23, 8432-8444.

Kim, S.G., Ugurbil, K., Strick, P.L., 1994. Activation of a cerebellar output nucleus during cognitive processing. Science 265, 949-951. http://doi.org/10.1126/science.8052851

Kishore, A., Meunier, S., Popa, T., 2014. Cerebellar influence on motor cortex plasticity: behavioral implications for Parkinson's disease. Front Neurol 5, 68. http://doi.org/10.3389/fneur.2014.00068

Krook-Magnuson, E., Szabo, G.G., Armstrong, C., Oijala, M., Soltesz, I., 2014. Cerebellar Directed Optogenetic Intervention Inhibits Spontaneous Hippocampal Seizures in a Mouse Model of Temporal Lobe Epilepsy. eNeuro 1. http://doi.org/10.1523/ENEURO.0005-14.2014

Lee, H.J., Weitz, A.J., Bernal-Casas, D., Duffy, B.A., Choy, M., Kravitz, A.V., Kreitzer, A.C., Lee, J.H., 2016. Activation of Direct and Indirect Pathway Medium Spiny Neurons Drives Distinct Brain-wide Responses. Neuron 91, 412-424. http://doi.org/10.1016/j.neuron.2016.06.010

Lee, J.H., 2012. Informing brain connectivity with optogenetic functional magnetic resonance imaging. Neuroimage 62, 2244-2249. http://doi.org/10.1016/j.neuroimage.2012.01.116

Lee, J.H., Durand, R., Gradinaru, V., Zhang, F., Goshen, I., Kim, D.S., Fenno, L.E., Ramakrishnan, C., Deisseroth, K., 2010. Global and local fMRI signals driven by neurons defined optogenetically by type and wiring. Nature 465, 788-792. http://doi.org/10.1038/nature09108

Lee, K.H., Mathews, P.J., Reeves, A.M., Choe, K.Y., Jami, S.A., Serrano, R.E., Otis, T.S., 2015. Circuit mechanisms underlying motor memory formation in the cerebellum. Neuron 86, 529-540. http://doi.org/10.1016/j.neuron.2015.03.010

Leong, A.T.L., Chan, R.W., Gao, P.P., Chan, Y.-S., Tsia, K.K., Yung, W.-H., Wu, E.X., 2016. Long-range projections coordinate distributed brain-wide neural activity with a specific spatiotemporal profile. Proceedings of the National Academy of Sciences 113, E8306-E8315. http://doi.org/10.1073/pnas.1616361113

Lin, Z.C., Tao, J., Gao, Y.L., Yin, D.Z., Chen, A.Z., Chen, L.D., 2014. Analysis of central mechanism of cognitive training on cognitive impairment after stroke: Resting-state functional magnetic resonance imaging study. J Int Med Res 42, 659-668. http://doi.org/10.1177/0300060513505809

Liu, W., Zhang, Y., Yuan, W., Wang, J., Li, S., 2012. A direct hippocampo-cerebellar projection in chicken. Anat Rec (Hoboken) 295, 1311-1320. http://doi.org/10.1002/ar.22515

Liu, Z., Xu, C., Xu, Y., Wang, Y., Zhao, B., Lv, Y., Cao, X., Zhang, K., Du, C., 2010. Decreased regional homogeneity in insula and cerebellum: A resting-state fMRI study in patients with major depression and subjects at high risk for major depression. Psychiatry Research: Neuroimaging 182, 211-215. http://doi.org/10.1016/j.pscychresns.2010.03.004

Lynch, J.C., Hoover, J.E., Strick, P.L., 1994. Input to the primate frontal eye field from the substantia nigra, superior colliculus, and dentate nucleus demonstrated by transneuronal transport. Exp Brain Res 100, 181-186. http://doi.org/10.1007/BF00227293

Madisen, L., Mao, T., Koch, H., Zhuo, J.M., Berenyi, A., Fujisawa, S., Hsu, Y.W., Garcia, A.J., 3rd, Gu, X., Zanella, S., Kidney, J., Gu, H., Mao, Y., Hooks, B.M., Boyden, E.S., Buzsaki, G., Ramirez, J.M., Jones, A.R., Svoboda, K., Han, X., Turner, E.E., Zeng, H., 2012. A toolbox of Cre-dependent optogenetic transgenic mice for light-induced activation and silencing. Nat Neurosci 15, 793-802. http://doi.org/10.1038/nn.3078

Magnuson, M.E., Thompson, G.J., Pan, W.J., Keilholz, S.D., 2014. Time-dependent effects of isoflurane and dexmedetomidine on functional connectivity, spectral characteristics, and spatial distribution of spontaneous BOLD fluctuations. NMR Biomed 27, 291-303. http://doi.org/10.1002/nbm.3062

Manni, E., Petrosini, L., 2004. A century of cerebellar somatotopy: a debated representation. Nat Rev Neurosci 5, 241-249. http://doi.org/10.1038/nrn1347

Massion, J., Rispal-Padel, L., 1972. Spatial organization of the cerebello-thalamo-cortical pathway. Brain Res 40, 61-65. http://doi.org/10.1016/0006-8993(72)90107-2

McGlinchey-Berroth, R., Carrillo, M.C., Gabrieli, J.D., Brawn, C.M., Disterhoft, J.F., 1997. Impaired trace eyeblink conditioning in bilateral, medial-temporal lobe amnesia. Behav Neurosci 111, 873-882. http://doi.org/10.1037/0735-7044.111.5.873

Middleton, F.A., Strick, P.L., 1994. Anatomical evidence for cerebellar and basal ganglia involvement in higher cognitive function. Science 266, 458-461. http://doi.org/10.1126/science.7939688

Middleton, F.A., Strick, P.L., 2001. Cerebellar projections to the prefrontal cortex of the primate. J Neurosci 21, 700-712.

Mushiake, H., Strick, P.L., 1993. Preferential activity of dentate neurons during limb movements guided by vision. J Neurophysiol 70, 2660-2664. http://doi.org/doi/pdf/10.1152/jn.1993.70.6.2660

Newman, P.P., Reza, H., 1979. Functional relationships between the hippocampus and the cerebellum: an electrophysiological study of the cat. J Physiol 287, 405-426. http://doi.org/10.1113/jphysiol.1979.sp012667

Nguyen-Vu, T.D.B., Kimpo, R.R., Rinaldi, J.M., Kohli, A., Zeng, H., Deisseroth, K., Raymond, J.L., 2013. Cerebellar Purkinje cell activity drives motor learning. Nat Neurosci 16, 1734-1736. http://doi.org/10.1038/nn.3576

Ohmae, S., Medina, J.F., 2015. Climbing fibers encode a temporal-difference prediction error during cerebellar learning in mice. Nat Neurosci 18, 1798-1803. http://doi.org/10.1038/nn.4167

Ohyama, T., Nores, W.L., Murphy, M., Mauk, M.D., 2003. What the cerebellum computes. Trends Neurosci 26, 222-227. http://doi.org/10.1016/S0166-2236(03)00054-7

Oscarsson, O., Uddenberg, N., 1964. Identification of a Spinocerebellar Tract Activated from Forelimb Afferents in the Cat. Acta Physiol Scand 62, 125-136. http://doi.org/10.1111/j.1748-1716.1964.tb03960.x

Pachitariu, M., Steinmetz, N., Kadir, S., Carandini, M., Harris, K.D., 2016. Kilosort: realtime spike-sorting for extracellular electrophysiology with hundreds of channels. bioRxiv. http://doi.org/10.1101/061481

Paleja, M., Girard, T.A., Herdman, K.A., Christensen, B.K., 2014. Two distinct neural networks functionally connected to the human hippocampus during pattern separation tasks. Brain Cogn 92c, 101-111. http://doi.org/10.1016/j.bandc.2014.10.009

Parker, K.L., Kim, Y.C., Kelley, R.M., Nessler, A.J., Chen, K.H., Muller-Ewald, V.A., Andreasen, N.C., Narayanan, N.S., 2017. Delta-frequency stimulation of cerebellar projections can compensate for schizophrenia-related medial frontal dysfunction. Mol Psychiatry 22, 647-655. http://doi.org/10.1038/mp.2017.50

Proville, R.D., Spolidoro, M., Guyon, N., Dugue, G.P., Selimi, F., Isope, P., Popa, D., Lena, C., 2014. Cerebellum involvement in cortical sensorimotor circuits for the control of voluntary movements. Nat Neurosci 17, 1233-1239. http://doi.org/10.1038/nn.3773

Rastogi, A., Ghahremani, A., Cash, R., 2015. Modulation of cerebello-cerebral resting state networks by site-specific stimulation. J Neurophysiol 114, 2084-2086. http://doi.org/10.1152/jn.00977.2014

Rochefort, C., Arabo, A., Andre, M., Poucet, B., Save, E., Rondi-Reig, L., 2011. Cerebellum shapes hippocampal spatial code. Science 334, 385-389. http://doi.org/10.1126/science.1207403

Ryali, S., Shih, Y.Y., Chen, T., Kochalka, J., Albaugh, D., Fang, Z., Supekar, K., Lee, J.H., Menon, V., 2016. Combining optogenetic stimulation and fMRI to validate a multivariate dynamical systems model for estimating causal brain interactions. Neuroimage 132, 398-405. http://doi.org/10.1016/j.neuroimage.2016.02.067

Sagar, S.M., Sharp, F.R., Curran, T., 1988. Expression of c-fos protein in brain: metabolic mapping at the cellular level. Science 240, 1328-1331. http://doi.org/10.1126/science.3131879

Schlerf, J.E., Verstynen, T.D., Ivry, R.B., Spencer, R.M., 2010. Evidence of a novel somatopic map in the human neocerebellum during complex actions. J Neurophysiol 103, 3330-3336. http://doi.org/10.1152/jn.01117.2009

Schmahmann, J.D., 1996. From movement to thought: anatomic substrates of the cerebellar contribution to cognitive processing. Hum Brain Mapp 4, 174-198. http://doi.org/10.1002/(sici)1097-0193(1996)4:3<174::aid-hbm3>3.0.co;2-0

Schmahmann, J.D., 2000. The role of the cerebellum in affect and psychosis. Journal of Neurolinguistics 13, 189-214. http://doi.org/dx.doi.org/10.1016/S0911-6044(00)00011-7

Schmahmann, J.D., 2004. Disorders of the cerebellum: ataxia, dysmetria of thought, and the cerebellar cognitive affective syndrome. J Neuropsychiatry Clin Neurosci 16, 367-378. http://doi.org/10.1176/jnp.16.3.367

Schmahmann, J.D., Pandya, D.N., 1997. Anatomic organization of the basilar pontine projections from prefrontal cortices in rhesus monkey. J Neurosci 17, 438-458.

Schmahmann, J.D., Rosene, D.L., Pandya, D.N., 2004. Motor projections to the basis pontis in rhesus monkey. J Comp Neurol 478, 248-268. http://doi.org/10.1002/cne.20286

Schmahmann, J.D., Sherman, J.C., 1997. Cerebellar cognitive affective syndrome. Int Rev Neurobiol 41, 433-440. http://doi.org/10.1016/S0074-7742(08)60363-3

Schmid, F., Wachsmuth, L., Albers, F., Schwalm, M., Stroh, A., Faber, C., 2016. True and apparent optogenetic BOLD fMRI signals. Magn Reson Med. http://doi.org/10.1002/mrm.26095

Shobe, J.L., Claar, L.D., Parhami, S., Bakhurin, K.I., Masmanidis, S.C., 2015. Brain activity mapping at multiple scales with silicon microprobes containing 1,024 electrodes. J Neurophysiol 114, 2043-2052. http://doi.org/10.1152/jn.00464.2015

Smith, S.M., 2002. Fast robust automated brain extraction. Hum Brain Mapp 17, 143-155. http://doi.org/10.1002/hbm.10062

Smith, S.M., Jenkinson, M., Woolrich, M.W., Beckmann, C.F., Behrens, T.E., Johansen-Berg, H., Bannister, P.R., De Luca, M., Drobnjak, I., Flitney, D.E., Niazy, R.K., Saunders, J., Vickers, J., Zhang, Y., De Stefano, N., Brady, J.M., Matthews, P.M., 2004. Advances in functional and structural MR image analysis and implementation as FSL. Neuroimage 23 Suppl 1, S208-219. http://doi.org/10.1016/j.neuroimage.2004.07.051

Solomon, P.R., Vander Schaaf, E.R., Thompson, R.F., Weisz, D.J., 1986. Hippocampus and trace conditioning of the rabbit's classically conditioned nictitating membrane response. Behav Neurosci 100, 729-744. http://doi.org/10.1037/0735-7044.100.5.729

Stujenske, J.M., Likhtik, E., Topiwala, M.A., Gordon, J.A., 2014. Fear and safety engage competing patterns of theta-gamma coupling in the basolateral amygdala. Neuron 83, 919-933. http://doi.org/10.1016/j.neuron.2014.07.026

Thach, W.T., 1975. Timing of activity in cerebellar dentate nucleus and cerebral motor cortex during prompt volitional movement. Brain Res 88, 233-241. http://doi.org/10.1016/0006-8993(75)90387-X

Waldvogel, D., van Gelderen, P., Muellbacher, W., Ziemann, U., Immisch, I., Hallett, M., 2000. The relative metabolic demand of inhibition and excitation. Nature 406, 995-998. http://doi.org/10.1038/35023171

Weiss, C., Bouwmeester, H., Power, J.M., Disterhoft, J.F., 1999. Hippocampal lesions prevent trace eyeblink conditioning in the freely moving rat. Behav Brain Res 99, 123-132. http://doi.org/10.1016/S0166-4328(98)00096-5

Weitz, A.J., Fang, Z., Lee, H.J., Fisher, R.S., Smith, W.C., Choy, M., Liu, J., Lin, P., Rosenberg, M., Lee, J.H., 2015. Optogenetic fMRI reveals distinct, frequency-dependent networks recruited by dorsal and intermediate hippocampus stimulations. Neuroimage 107, 229-241. http://doi.org/10.1016/j.neuroimage.2014.10.039

Woolrich, M., 2008. Robust group analysis using outlier inference. Neuroimage 41, 286-301. http://doi.org/10.1016/j.neuroimage.2008.02.042

Yeo, C.H., Hardiman, M.J., Glickstein, M., 1985. Classical conditioning of the nictitating membrane response of the rabbit. I. Lesions of the cerebellar nuclei. Exp Brain Res 60, 87-98.

Yu, W., Krook-Magnuson, E., 2015. Cognitive Collaborations: Bidirectional Functional Connectivity Between the Cerebellum and the Hippocampus. Front Syst Neurosci 9, 177. http://doi.org/10.3389/fnsys.2015.00177

Zhang, Y., Brady, M., Smith, S., 2001. Segmentation of brain MR images through a hidden Markov random field model and the expectation-maximization algorithm. IEEE Trans Med Imaging 20, 45-57. http://doi.org/10.1109/42.906424

Table 1. Summary of *in vivo* electrophysiology data.

A. Percent of all cells modulated by stimulus

Stimulus Type	Response Type	Mean (%) ± SEM	n (mice)
5Hz, 143mW/mm^2, 100ms	*Excited*	62 ± 15	3
	Inhibited	19 ± 10	3
	Mixed	8 ± 4	3
5Hz, 143mW/mm^2, 25ms	*Excited*	13 ± 7	3
	Inhibited	3 ± 2	3
	Mixed	0 ± 0	3
10Hz, 143mW/mm^2, 50ms	*Excited*	33 ± 4	3
	Inhibited	6 ± 1	3
	Mixed	5 ± 3	3
20Hz, 143mW/mm^2, 25ms	*Excited*	38 ± 7	3
	Inhibited	12 ± 2	3
	Mixed	2 ± 2	3
5Hz, 10mW/mm^2, 100ms	*Excited*	21 ± 6	3
	Inhibited	8 ± 5	3
	Mixed	1 ± 1	3
5Hz, 38mW/mm^2, 100ms	*Excited*	11 ± 5	3
	Inhibited	9 ± 4	3
	Mixed	0 ± 0	3

B. Peak response (maximum increase in baseline-normalized firing rate (<4 s))

Stimulus Type	Response Type	Mean (s) ± SEM	n (cells)
5Hz, 143mW/mm^2, 100ms	*Excited*	4.83 ± 0.45	64
10Hz, 143mW/mm^2, 50ms	*Excited*	4.76 ± 0.47	47
20Hz, 143mW/mm^2, 25ms	*Excited*	3.21 ± 0.50	27
5Hz, 10mW/mm^2, 100ms	*Excited*	2.00 ± 0.25	18
5Hz, 38mW/mm^2, 100ms	*Excited*	4.57 ± 1.07	11

C. Sustained response (average change over baseline firing rate between 10-20s after stimulus onset)

Stimulus Type	Response Type	Mean ± SEM	n (cells)
5Hz, 143mW/mm^2, 100ms	*Excited*	1.94 ± 0.22	69
	Inhibited	-0.63 ± 0.07	22
10Hz, 143mW/mm^2, 50ms	*Excited*	0.28 ± 0.45	27
	Inhibited	-0.56 ± 0.07	10
20Hz, 143mW/mm^2, 25ms	*Excited*	0.28 ± 0.09	27
	Inhibited	-0.55 ± 0.08	12
5Hz ,10mW/mm^2, 100ms	*Excited*	0.48 ± 0.13	18
	Inhibited	-0.63 ± 0.11	9
5Hz, 38mW/mm^2, 100ms	*Excited*	0.99 ± 0.38	12
	Inhibited	-0.63 ± 0.13	9

Table 2. Quantification of BOLD changes in anatomical forebrain and midbrain regions.

Brain region (general function)	Contralateral to laser stimulation			Ipsilateral to laser stimulation			
	# activated voxels	Total # voxels in mask	% Activation	# activated voxels	Total # voxels in mask	% Activation	Laterality Index
Thalamus (motor and sensory)	208	452	**46**	51	360	**14**	**0.53**
Hippocampus (memory and navigation)	115	539	**21**	59	536	**11**	**0.32**
Reticular Formation (consciousness)	63	90	**70**	27	96	**28**	**0.43**
Motor Cortex (motor)	58	258	**22**	22	217	**10**	**0.38**
Anterior Cingulate Cortex (executive and cognitive)	34	134	**25**	23	124	**19**	**0.16**
Retrosplenial Cortex (cognition, memory, and navigation)	29	128	**23**	35	156	**22**	**0.00**
Somatosensory Cortex (sensory)	28	591	**5**	5	622	**0.8**	**0.71**
Limbic Cortices (emotion)	26	35	**74**	8	32	**25**	**0.50**
Basal Ganglia (cognition and movement)	8	552	**2**	1	588	**0.17**	**0.79**
Rhinal Cortex (memory and navigation)	0	329	**0**	35	357	**10**	**-1.00**
Insular Cortex (sensory)	0	127	**0**	0	130	**0**	**0.00**

Midline brain structures							
Periaqueductal Gray (pain)	77	203	**38**
Septal Nuclei (emotion)	35	121	**29**
Hypothalamus (physiological control)	0	383	**1**

Figure 4

Figure 6

Figure 1

A

Arch-GFP in PNs

1 mm

0.5 mm

0.5 mm

B

Steady-state suppresion of output

Purkinje Neurons → Cerebellar Nuclei → Forebrain

Transient, light-induced output of cerebellum

Light

Purkinje Neurons → Cerebellar Nuclei → Forebrain

C

fiber optic cannula

Cerebellum
Inferior Colliculus
Superior Colliculus
Cerebral Cortex
corpus callosum
Hippoc
LV
Septum
Olfactory Bulb
Midbrain
Thalamus
Spinal Cord
Medulla
Pons
Hypothalamus
Preoptic Area

D

Optic fiber implant

1 mm

Bregma -6.5 mm

1 mm

Figure 2

A

Arch > Control

5 Hz   10 Hz   20 Hz

B

5 Hz   10 Hz   20 Hz

% BOLD Change

0.6

0.3

0

-0.3

Arch
Control

0   30

Time from light onset (s)

C

5 Hz   10 Hz   20 Hz

Cells

0   30

Time from light onset (s)

10+

5

0

Fold change

D

5 Hz   10 Hz   20 Hz

Fold change

6

0

Excited
Inhibited

0   30

Time from light onset (s)

E

Percent of Cells Modulated

100

50

0

*
*

Excited
Inhibited
Mixed

5   10   20

Initial Peak (ΔR)

20

0

*

5   10   20

Stimulation Frequency (Hz)

Sustained (ΔR)

8

4

0

****
****

5   10   20

Figure 3

Figure 5